Photoelectron microscopy

2001 J. Phys.: Condens. Matter 13 11391

(http://iopscience.iop.org/0953-8984/13/49/316)

INSTITUTE OF PHYSICS PUBLISHING JOURNAL OF PHYSICS: CONDENSED MATTER

J. Phys.: Condens. Matter **13** (2001) 11391–11404 PII: S0953-8984(01)28786-4

Photoelectron microscopy

E Bauer

Department of Physics and Astronomy, Arizona State University, Tempe, AZ 85287-1504, USA

Received 20 September 2001
Published 10 December 2001
Online at stacks.iop.org/JPhysCM/13/11391

Abstract

The physical principles, the experimental realization, the methodology and the application of synchrotron radiation-induced non-scanning photoemission electron microscopy (XPEEM) are discussed, including the combination with low-energy electron microscopy and the corresponding diffraction and spectroscopy techniques. Standard XPEEM that uses the slow secondaries for imaging is extended to imaging with energy-selected electrons by the addition of an imaging energy filter that allows to select photoelectrons, Auger electrons or a narrow energy window in the secondary-electron distribution. This combination of techniques leads to spectroscopic photoemission and low-energy electron microscopy (SPELEEM) which allows a comprehensive characterization of surfaces and thin films on the 10 nm scale.

(Some figures in this article are in colour only in the electronic version)

1. Introduction

More than a decade after the pioneering work of Tonner and Harp [1], synchrotron radiation-induced photoemission electron microscopy (XPEEM) is now a well-established technique. Most work done up to now made use of the slow secondary electrons created in the photoionization process and impressive results have already been achieved in this imaging mode, for example the imaging of the domain structure of antiferromagnetic materials with x-ray magnetic linear dichroism (XMLD) contrast [2]. In order to obtain good spatial resolution in this imaging mode, the wide energy distribution of the slow secondaries has to be reduced by decreasing the angular aperture of the imaging beam considerably at the expense of the transmitted intensity. An alternative imaging mode, imaging with energy-selected Auger or photoelectrons, was suggested some time ago [3,4] but only became viable with the availability of third-generation synchrotron radiation sources with high brightness. It resulted from the desire to add a chemically sensitive imaging mode to the structurally sensitive imaging with slow reflected electrons (LEEM). Originally, Auger emission electron microscopy (AEEM) excited by electrons was the only realistic possibility because of the high current densities that could be achieved in electron beams, but the advent of undulators changed the situation clearly in favour of XPEEM. Not only are the linewidths and the background much smaller

in the case of photoelectrons than in the case of Auger electrons, but also the influence of the chemical bonding is much more easily accessible and the electron energy can be changed by changing the photon energy. Today this combination of spectroscopic imaging with LEEM is therefore nearly exclusively achieved using photoelectrons. In this paper we review the various imaging, diffraction and spectroscopy modes possible with XPEEM, LEEM and SPELEEM (section 2), describe some of the instrumental aspects (section 3) and give a few illustrations of their possibilities (section 4). A brief outlook (section 5) concludes this contribution.

2. Basic physics of the imaging, diffraction and spectroscopy modes

With photon irradiation, photoelectrons, Auger electrons and secondary electrons may be used; with electron irradiation, elastically and inelastically scattered electrons, Auger electrons and secondary electrons may be used. The choice of the imaging, diffraction or spectroscopy mode depends upon the information desired: structural, chemical, magnetic or electronic, from the topmost layers or from deeper layers.

Structural information from crystalline samples is best obtained with LEEM. At low energies, usually less than 50 eV, it gives images with high brightness and good resolution due to the concentration of the reflected intensity into diffracted beams and the high reflection coefficient of many materials, in particular at very low energies ($<$10 eV). The information depth of LEEM is determined in part by the inelastic mean free path, which rises in many materials with decreasing energy from a minimum of about 0.3 nm at about 50 eV well into the 1 nm range in the 1 eV range, and in part by the elastic mean free path, which frequently determines the information depth at very low energies. This is the case when band gaps exist above the vacuum level. On the other hand, if there is a high density of unoccupied electronic states at low energies, starting from the Fermi level, inelastic scattering into these states can be decisive and reduce the information depth to less than 1 nm, even to a few 0.1 nm.

In addition to the diffraction contrast due to the periodic arrangement of the atoms in the sample, there is also a phase contrast due to the geometry of the sample that allows imaging of monatomic steps and atomic thickness discrimination between atomically flat regions in thin films. The lateral resolution in present instruments is below 10 nm, the image brightness in many cases such that image acquisition at video rates is possible. This makes LEEM an ideal tool for the study of surface processes that are accompanied by changes in reflectivity or—at very low energies—by changes of the work function. One limitation of LEEM at very low energies that is inherent to all imaging methods that use cathode lenses is the field distortion caused by surface asperities and by strong local work function changes. This is particularly evident in mirror microscopy in which the electrons are reflected in the potential distribution in front of the sample. This gives a distorted impression of the sample (size, contrast distribution). However, the shadow and diffraction effects from surface asperities due to the oblique incidence of the light in XPEEM are absent in LEEM, where the incident and reflected beam are (nearly) perpendicular to the surface. In all cases in which the surface is chemically homogeneous or in which the chemical composition and bonding is known, LEEM is far superior to XPEEM because of the inherent higher resolution and shorter image acquisition time. In particular, on surfaces that are too flat to produce contrast via shadowing, LEEM is the only method to produce contrast via diffraction—for example on the clean Si(100) surface with its two (2×1) domains—or via geometric phase contrast—for example on clean surfaces with monatomic steps. More information on LEEM, including its physical basis, may be found in [5] and [6].

On the other hand, whenever a surface is chemically heterogeneous and this heterogeneity is to be imaged, XPEEM is the best method. In principle, electron energy loss microscopy that

is possible in a LEEM instrument equipped with a band pass filter could be used also—as is done in transmission electron microscopy—but the characteristic core shell losses have such a low intensity compared to the background that this method cannot compete with XPEEM imaging. The frequently strong and well-defined plasmon losses are not suitable for chemical imaging because they are not sufficiently material-specific. The only methods based on incident electrons that appear viable are appearance potential electron microscopy (APEM) and AEEM. In APEM, images are taken below, at and above an inner shell ionization energy and properly subtracted. The elastically backscattered intensity is usually too low at the energies of interest, so the change of the secondary electron yield has to used for imaging, similarly to the case for XPEEM without an energy filter. AEEM was shown to be feasible with emission energies as high as 350 eV [7], but XPEEM with undulator radiation and band pass electron energy filters made these methods obsolete, as already mentioned in the introduction. This makes XPEEM the chemical imaging method of choice.

Chemical imaging with XPEEM can be done either with secondary electrons or with photoelectrons. Auger electrons could in principle be used too, but they are less useful than photoelectrons because they contain a convolution of two states, and the peaks are usually broader in energy and are situated on a higher background than the photoelectron peaks. As a consequence they are used only in special situations that will be discussed below. In the past, most XPEEM work was done with secondary electrons because none of the high-resolution instruments except the SPELEEM had an imaging band pass energy filter. Secondary electron imaging uses the slow secondaries that are produced in the filling of the core hole created in the primary photoexcitation processes. These processes have a particularly sharp onset in s and p core levels and depend upon the transition probability from the ground state to the unoccupied states above the Fermi level. Three aspects of the transition probability are of particular importance: (i) its sensitivity to chemical bonding which is used in near-edge absorption fine structure (NEXAFS) imaging, mainly of organic materials; (ii) its dependence upon the spin-dependent density of states in the case of circular polarized light which is the basis of x-ray circular dichroism imaging (XMCD imaging); (iii) the dependence of the absorption of linear polarized light on charge distribution anisotropy, either due to molecular orientation or induced by spin–orbit interaction in antiferromagnetics. This is the basis of magnetic linear dichroism (XMLD) imaging of antiferromagnetics. Of course, independently of these special applications, the sudden increase of the secondary electron emission at the excitation threshold generally allows identification of the chemical species imaged.

Secondary electron emission imaging has at least two advantages over photoelectron imaging whenever that it possible too: (i) it does not require a band-pass filter and (ii) the surrounding of the species to be imaged acts as a secondary multiplier. The second advantage is, however, useful only if the excitation thresholds of the surrounding are higher than that of the species to be imaged, otherwise the surrounding produces too strong a secondary electron background. The energy distribution of secondary electrons is wide, usually several eV FWHM. Because of the chromatic aberration of the objective lens, the spatial resolution is therefore poor without a band pass filter or aberration corrector. The procedure used up to now, the reduction of the contribution of the faster electrons to the signal by an aperture in the crossover of the secondary electrons in the focal plane of the objective lens or an image plane of it, of course improves the resolution but at the same time reduces transmission considerably [8, 9]. Whenever photoelectron imaging can be used, it has at least two advantages over secondary electron imaging: (i) a narrow energy distribution ranging from less than $\frac{1}{2}$ eV to about 2 eV for useful inner shells and (ii) an easier determination of the bonding via the associated ‘chemical’ shift of the binding energy of the core level.

Irrespective of lateral resolution, signal and signal/background ratio, there is one consideration which in many cases determines which electrons should be used: the information depth. If a large information depth is desired, then a look at the so-called 'universal curve' of the inelastic mean free path [10] shows that secondary electrons with energies between 0 and about 5 eV are the best choice; if a high surface sensitivity is needed, then photoelectrons with energies near the minimum of the inelastic mean free path should be used. This can be easily achieved for any binding energy by choosing photon energies 30–100 eV above the ionization energy. In many cases the maximum of the ionization cross section is in this energy range, so in these cases the surface sensitivity is optimized in a twofold manner.

It is well known that the inelastic mean free paths of many materials deviate strongly from the 'universal curve'. In insulators in which the low energy excitations are missing, they can be significantly larger. In materials with a high density of states above the Fermi level such as d and f metals and alloys, strong low-energy excitations occur at low energies that strongly reduce the inelastic mean free path [11]. In ferromagnetic materials—that is, in materials in which the densities of unoccupied majority and minority spin electron states differ significantly—the inelastic mean free paths are spin dependent [12]. This could be important for the understanding of the contrast in x-ray magnetic dichroism imaging, in addition to the spin-dependent excitation probability.

Magnetic imaging with secondary electrons—that is, XMCDPEEM for ferromagnetic materials and XMLDPEEM for antiferromagnetic materials—is one of the main applications of XPEEM. Compared to other magnetic imaging methods with slow electrons such as scanning electron microscopy with polarization analysis (SEMPA) or spin-polarized low energy electron microscopy (SPLEEM), it has the advantage of chemical sensitivity and allows separation of spin and orbital magnetic moments. In addition, it does not require the spin-sensitive detector or spin-polarized electron source that are needed in SEMPA and SPLEEM, respectively. The first magnetic XPEEM images with secondary electrons [13] were actually obtained with a very simple instrument [14]. Auger electrons may also be used for magnetic imaging as first demonstrated with an imaging energy analyser [15, 16]. In both cases the magnetic signal, the so-called MCD asymmetry $A = (I_+ - I_-)/(I_+ + I_-)$ is proportional to $\boldsymbol{M} \cdot \boldsymbol{\sigma}$ where $\boldsymbol{M}$ is the sample magnetization, $\boldsymbol{\sigma}$ the photon spin and I_+, I_- the photoemission intensities for opposite helicities of the circular polarization. The magnetic contrast in XMLDPEEM arises from the fact that absorption of x-rays with the electric vector parallel to the ellipsoidal charge distribution caused by spin–orbit interaction is different from that perpendicular to it. Instead of differences between the two $\boldsymbol{\sigma}$- or $\boldsymbol{E}$-directions, frequently image ratios are also used. Photoelectrons also carry magnetic information that depends, however, in a more complicated manner upon $\boldsymbol{M}$, $\boldsymbol{\sigma}$ and the emission direction.

Electronic imaging—that is, imaging with energy-selected photoelectrons from the valence band—is usually less suitable for chemical identification unless the valence band contains regions with a high density of states such as in d and f electron systems. The information of interest is in general not in the real-space image but in the reciprocal-space image. This is at fixed photon energy $h\nu$ and selected photoelectron energy E, to a first approximation, a cut through the band structure at the binding energy $E_B = h\nu - E - \phi$ (ϕ = work function). This 'band-structure mapping' requires a band-pass filter with good energy resolution. A quantitative analysis has to take transition matrix elements and photoelectron diffraction into account.

Photoelectron diffraction (PED, XPD), like low energy electron diffraction (LEED), gives information on the reciprocal space, but with essential differences: (i) in LEED there is a plane wave incident from outside the crystal while in PED the 'incident' wave is the spherical wave of the photoelectron emitted from the ionized atom inside the crystal; (ii) LEED is sensitive

to long-range order while PED is sensitive to the environment of the ionized atom—that is, it is sensitive to short-range order; (iii) it is in general difficult to extract chemical information from LEED while in PED the energy of the photoelectron is characteristic for the emitting atom. PED with circularly polarized light allows direct short-range structure determination in non-chiral and non-magnetic materials [17, 18]. PED and closely related photoelectron holography can be carried out in any XPEEM equipped with a band-pass filter.

Photoelectron spectroscopy (PES, XPS) is a by-product of any PEEM with a band pass filter. Spectra can be obtained either by integrating the intensity in small regions of a series of images taken at many photoelectron energies or by selecting the desired region of the sample with a field-limiting aperture and imaging the dispersive plane of the energy filter. The first method allows selection of very small regions but is time consuming, while the second one is fast but in general limited to somewhat larger regions. If only local spectra of very small regions are of interest, then microspectroscopy with zone plates is preferable because in this case the light intensity is focused into a fine spot as small as 30 nm in present-day scanning photoelectron microscopes (SPEMs) [19, 20]. For both XPS and XPD, the considerations regarding escape depths in connection with imaging are important.

3. Instrumentation

XPEEM instrumentation has developed rapidly during the last decade due to the increasing demands on resolution: bending magnets have been replaced increasingly by undulators in order to obtain the high brightness needed for high-resolution imaging and the microscopes have become more sophisticated. There are now three commercial electrostatic PEEM instruments suitable for XPEEM studies in the sub-100 nm range [21–23], several home-built XPEEMs [9,24], a commercial magnetic XPEEM with band-pass filter [21] and the SPELEEM, originally home-built [25] but now also commercially available [21]. The resolution, for all of these instruments, is limited by the chromatic and spherical aberration of the objective lens. This has stimulated the development of aberration-corrected instruments, the SMART at BESSY II [26, 27] and the PEEM III at ALS; at least the first of these should be in operation by the time this paper is published.

As far as the light source is concerned, variable-polarization undulators are now increasingly used which give a choice of any ellipticity from linear to circular polarization. This is important for many applications, whether it is magnetic or structural dichroism that is used for the contrast. The APPLE II (Sasaki) type of undulator [28] seems to be the most popular design, but other designs are also used [29–31]. For dichroism studies, easy helicity switching is important, which has already been achieved with an APPLE II undulator [32] up to 0.1 Hz.

All microscopes used today have at least three lenses: an objective, an intermediate and a projective lens. The intermediate lens allows switching between imaging of the real and the reciprocal space, that is between image and diffraction pattern or band-structure map. The objective lens, together with an angle-limiting aperture (‘contrast aperture’) in the diffraction plane determines the resolution and transmission of the system, provided that the instrument is well vibration damped and magnetically shielded against ac fields. Magnetic objectives are superior in resolution and transmission to the electrostatic objectives that are frequently used in the study of magnetic samples. However, with proper lens design the magnetic field at the position of the specimen can be reduced to negligible values. The projective lens provides the final magnification on the microchannel plate—fluorescent screen detector. The operation voltages of the microscopes range from 5 to 30 kV. In the electrostatic microscopes the sample is usually at ground potential, and in the magnetic microscopes at high potential. The best present

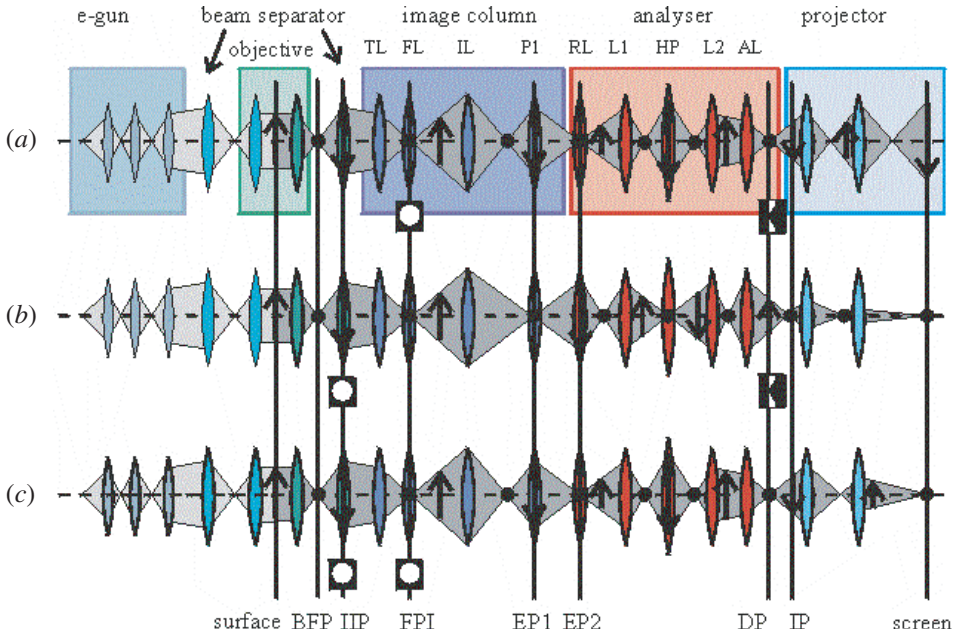

Figure 1. An optical schematic diagram of the SPELEEM [25]. For an explanation, see the text.

resolutions of the instruments are 7 nm in threshold microscopy with Hg high pressure arc light in a magnetic microscope and about 20 nm with synchrotron radiation-excited secondary electrons [9] and photoelectrons [25]. These general comments having been made, we can turn now to a more detailed description of the currently most sophisticated system, the SPELEEM.

As already mentioned in the introduction, the SPELEEM combines LEEM and energy-filtered XPEEM. LEEM requires a beam separator between the incident and reflected beam. For simplicity this is not shown in the optical schematic diagram of the instrument (figure 1) [25], but only indicated as a lens on both sides of the objective lens. Also not shown are the deflectors and stigmators. For XPEEM (*a*), XPD (*b*) and XPS (*c*) only the components to the right of the objective are relevant. The photon beam illuminates the sample at a grazing angle of incidence of 15°. The objective lens produces in its back focal plane, BFP, the diffraction pattern and in the centre of the beam separator a first intermediate image. The diffraction pattern is imaged by the transfer lens, TL, into the field lens, FL. The two lenses together produce a second intermediate image in front of the intermediate lens, IL. Up to that point the three operation modes do not differ except for the apertures indicated by squares with open circles. In XPEEM the angular aperture has to be limited by an aperture in the focal plane which is placed in its image plane, FPI, in order to reduce aberrations; in XPD the area contributing to the diffraction pattern has to be limited by a field-limiting aperture in the first intermediate image plane, IIP. Finally, in XPS both apertures are inserted in order to obtain good energy resolution (FPI) and to select the specimen region of interest (IIP).

Continuing now the optical path, the intermediate lens IL images the second intermediate image into the lens P1 and, together with P1, the diffraction pattern into the entrance plane EP2, (located in the retarding lens RL) of the energy filter, a 180° hemispherical analyser. In the analyser the electrons are retarded to 1/20 of their original energy and reaccelerated by the acceleration lens AL at its exit to their original energy again. The lenses in the analyser image the diffraction pattern into its dispersive plane DP. For XPEEM the energy-selection slit

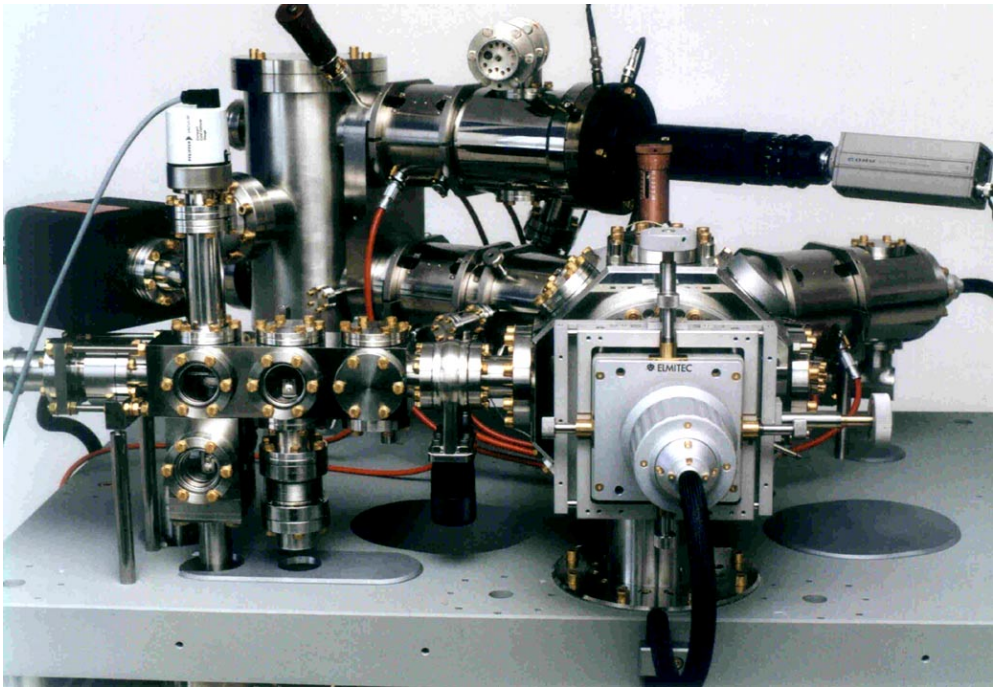

Figure 2. SPELEEM. Courtesy: C Koziol [21]. For an explanation, see the text.

is inserted here and the image in the image plane IP is magnified with a double projector onto the image detector. For XPS the energy-selection slit is removed and the double projector is set to image the dispersive plane onto the image detector. For XPD it is not the image that has to be filtered but the diffraction pattern. Accordingly, the intermediate lens (IL) is excited such that diffraction pattern and image are interchanged. Beyond the energy filter the lens settings are the same as in XPEEM. The desired energy is selected by changing the potential of the sample. Thus by changing three apertures and the excitation of two lenses it is possible to switch from one operation mode to the other.

This instrument is shown in figure 2. The LEEM illumination system is on the right at the back; the image column, analyser (vertical) and projector are on the left at the back. The centre front shows the specimen manipulator and the main chamber that houses the specimen and objective lens. Hidden behind it is the beam separator connecting illumination and image column. On the left at the front are the airlock, preparation chamber and sample transfer system. This instrument is not aberration corrected, so its resolution is limited to the high 1 nm—low 10 nm range. A significant improvement, not only in resolution but also in transmission, is expected from aberration-corrected systems. Figure 3 [27] shows the expected improvements for the case of the SMART instrument, but sub-nm resolutions at higher energies are unrealistic because of the low signal which requires either unacceptable image acquisition times or destructive photon flux densities.

4. Some applications of XPEEM

Much of the early work served mainly in the exploration of the application range of XPEEM. In addition to the early work on magnetic dichroism imaging, the orientation of polymer films,

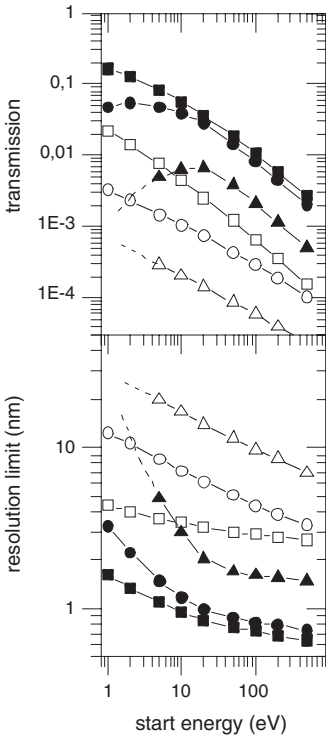

Figure 3. Theoretical transmission and resolution of the SMART objective without (open symbols) and with (full symbols) aberration correction for energy widths of 0.1 eV (squares), 1 eV (circles) and 5 eV (triangles) as a function of the start energy [27]. The data are from [33] and for the optimum aperture.

the phase separation in polymers, biological samples, lubricant layers on magnetic storage media and titanium silicides and other systems of interest in semiconductor technology were studied with secondary or total yield imaging. This kind of exploratory work is still in progress with the newer more powerful instruments, but some particularly successful applications have already become evident, the foremost of which is in the study of magnetic materials. An interesting special application of the lateral resolution of XPEEM is in the study of the thickness dependence of the magnetic properties of thin films using wedge-shaped films [34, 35]. Only moderate resolution is needed for this work for wedges with slowly increasing thickness. Studies with energy-filtering instruments such as the SPELEEM are still rare and have been concentrated on chemical imaging. The work with aberration-corrected instruments is still in the exploratory phase. In the following, some results from the currently best instruments will illustrate the recent work.

The first example illustrates an application of XPEEM with secondary electrons in biology. It explores to what extent Gd that is promising in neutron capture therapy for cancer is incorporated selectively in tumour cells. The study was made with the electrostatic MEPHISTO PEEM at the Wisconsin SRL [24]. Figure 4(*a*) shows the Ca distribution within some tumour cells grown on an Au substrate and exposed to a Gd marker; figure 4(*b*) shows local Gd absorption spectra taken simultaneously from various regions [36]. It is evident that the Ca concentration in the cell nucleus is lower than in the surrounding cytoplasm, while the reverse is true for the Gd concentration which is only 500 ppm. In this kind of work in which low concentrations have to be imaged, resolution has to be sacrificed to achieve sensitivity.

The second example is the imaging of antiferromagnetic (AFM) domains in thin epitaxial $LaFeO_3$ films via XMLD contrast that was achieved with the PEEM II instrument at ALS [2].

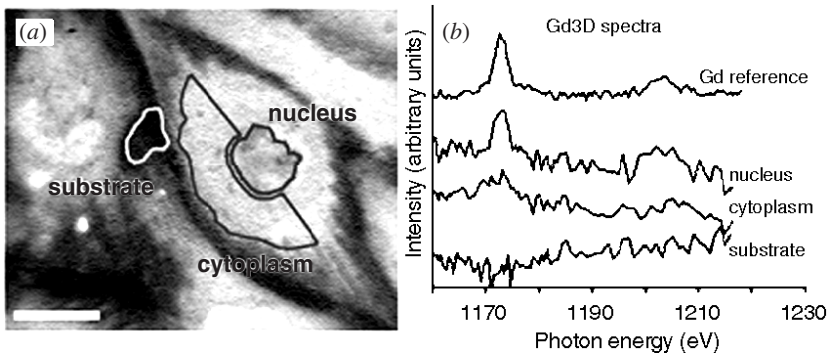

Figure 4. (*a*) A calcium distribution map in a group of tumour cells and (*b*) gadolinium 3d absorption spectra from the regions indicated and from a Gd reference [36].

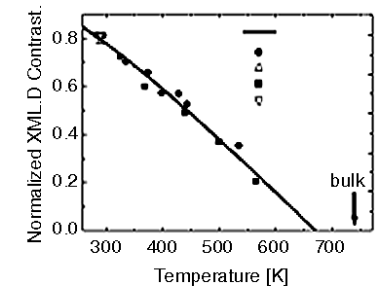

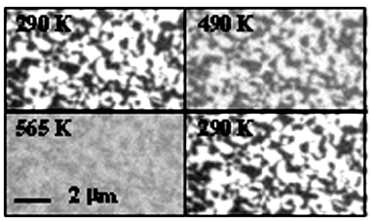

Figure 5. XMLDPEEM images of an epitaxial $LaFeO_3$ layer at various temperatures and the temperature dependence of the XMLD contrast which is a measure of the magnetization [2] (courtesy: J Stoehr).

The physical basis of the contrast formation is well explained in [37]. The lower part of figure 5 shows images taken at different temperatures during heating and cooling, the upper part the reversible temperature dependence of the AFM domain contrast. The theoretical fit extrapolates to a Néel temperature of 670, 70 K below that of the bulk material. Obviously, sub-100 nm resolution is necessary for good imaging of such small domains. Extension of this work, combining XMLD and XMCD imaging, has allowed to study the local coupling between the spins at the interface between $LaFeO_3$ and a thin Co layer [38], the so-called exchange bias that plays an important role in magnetic reading heads and memory cells. The AFM substrate was found to determine the local spin alignment of the Co. This local exchange bias was clearly seen in the local remanent hysteresis curves as characterized by the brightness of the domains after magnetic field application. The reverse effect, in which the ferromagnetic Co layer imposes its local spin orientation on that of the AFM NiO(100) single-crystal substrate, was also observed recently [39]. These examples demonstrate that dichroism imaging not only can image very small magnetic domains but also can give quantitative magnetic information in the sub-μm range.

Another application of dichroism imaging is in the study of magnetic micropatterns that

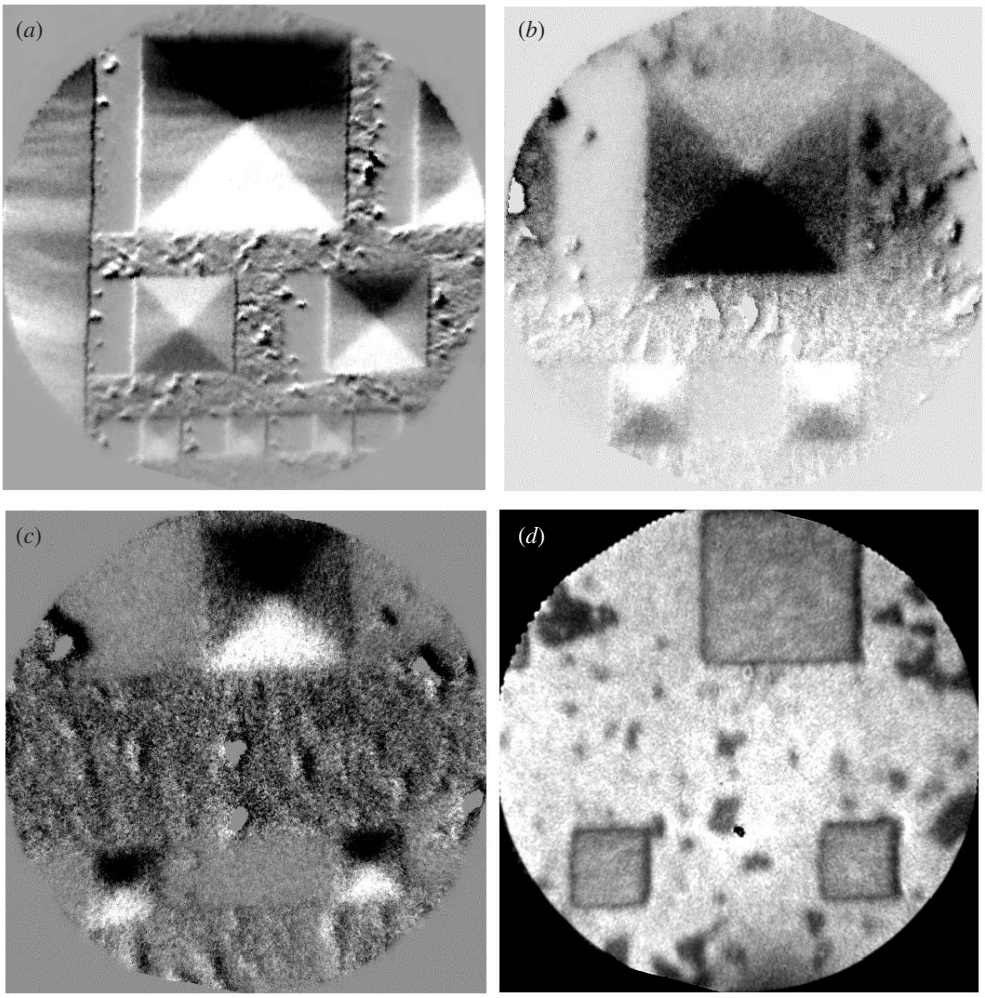

Figure 6. XMCDPEEM images ((*a*)–(*c*)) and a LEEM image (*d*) of permalloy squares prepared from a continuous film on Ag-covered Si by ion milling, taken at the Fe L_3 absorption edge. (*a*) 10 and 5 μm; (*b*) 5 and 2 μm; (*c*), (*d*) 2 and 1 μm squares [40].

are of interest for magnetic storage. This is illustrated in figures 6(*a*)–6(*c*) with XMCDPEEM images of small permalloy squares [40]. They were taken in a LEEM during the early commissioning phase of a new beamline at ELETTRA. The image shift between the images taken with opposite helicity was not corrected, but the closure domain structure is clearly seen even in the smallest pattern (1 μm^2). For comparison figure 6(*d*) shows also the corresponding LEEM image of the polycrystalline layer. The 50 nm diameter vortex core in the centre of the squares [41] could not be imaged because of the image shift, insufficient signal/noise ratio and resolution. Future improvements of the microscope (energy filter!) and of the beamline, however, are expected to eliminate these problems. Figure 7 is another illustration of the extraction of quantitative information from XMCDPEEM images. It shows the intensity of a 1 μm^2 region of a small epitaxial Co crystal on a W(110) surface extracted from secondary electron images taken at various photon energies near the Co L_3 absorption edge. From the

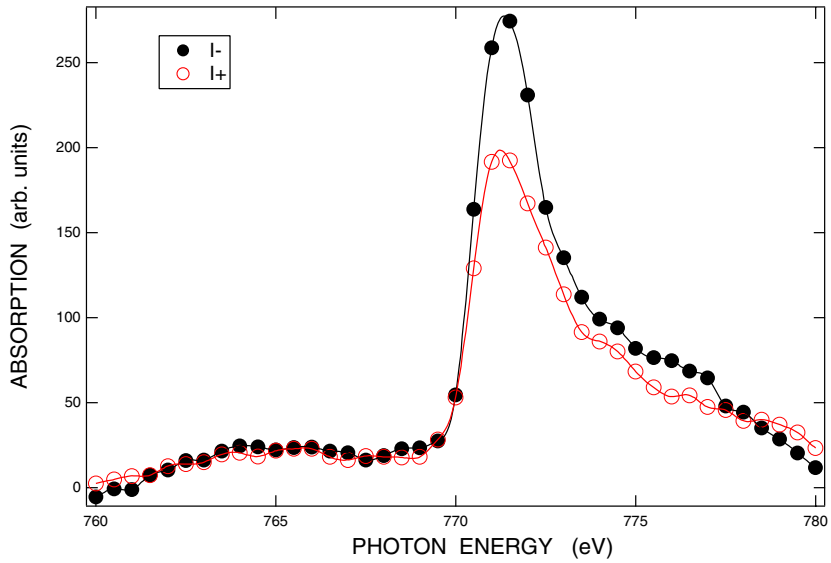

Figure 7. Co L_3 absorption spectra from 1 μm^2 regions of a small Co(0001)-oriented Co crystal on a W(110) single-crystal surface taken with light of opposite helicity. A background of 165 (arbitrary units) has been subtracted [40].

intensity difference between the images with opposite helicity a raw MCD asymmetry of $A = -0.18$ is extracted and after several corrections a final A-value of -0.28 [40] is obtained, in good agreement with literature data from lateral-averaging studies [42].

While magnetic imaging with secondary electrons via magnetic dichroism contrast can be done without an energy filter, though with limited resolution, chemical imaging with photoelectrons requires an energy filter. This can, in principle, be a high pass filter similar to that in standard LEED optics [43] with proper subtraction of images taken above and below the photoelectron energy of interest. However, the resolution is limited by the mesh size of the retarding grids that cannot be made very small without a large loss of transmission. The resulting image also suffers from the poor signal/noise ratio typical for high pass filters. For good signal/noise ratio and resolution a band pass filter is necessary. Such a photoelectron image and spectra, taken with the prototype SPELEEM, are shown in figure 8 [25]. After the completion of a monolayer, Pb grows on flat regions of a W(110) surface in large flat (111)-oriented crystals as seen on the left-hand side of the image. The local spectra from the indicated 0.25 μm^2 areas of the crystal and of the monolayer taken from many images show a Pb 5d peak FWHM of 0.5 eV and a chemical shift of 0.15 eV between crystal and monolayer. The spatial resolution is in this example about 70 nm.

An application of SPELEEM to the study of nanostructures is shown in figure 9. Two monolayers of InAs were deposited at 200 °C on Se-terminated GaAs which resulted in the formation of the nanocrystals seen in the LEEM image (*a*) and in the In 4d XPEEM image (*b*). A detailed analysis of the local In 4d, Ga 3d and Se 3d spectra of the nanocrystals and of the background revealed that the nanocrystals are not pure InAs crystals, but are covered by an $InGaSe_3$ layer [45]. More information on the possibilities and limitations of SPELEEM, in particular also in the PED and PES modes of operation, can be found in [25, 45, 46].

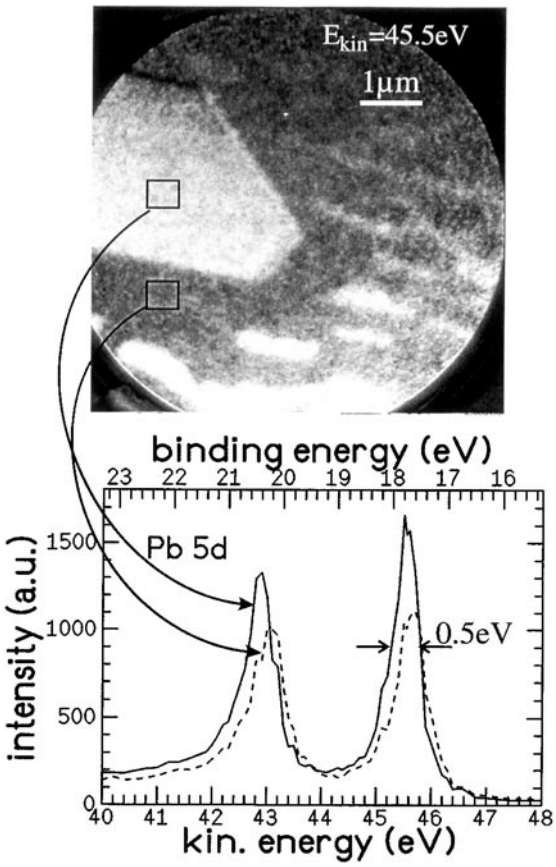

Figure 8. A Pb 5d photoelectron image of a Pb layer on a W(110) surface and photoelectron spectra obtained by integrating the intensity in the regions indicated. The photoelectron energy was changed in steps of 0.5–1 eV. The photon energy is 65 eV [25].

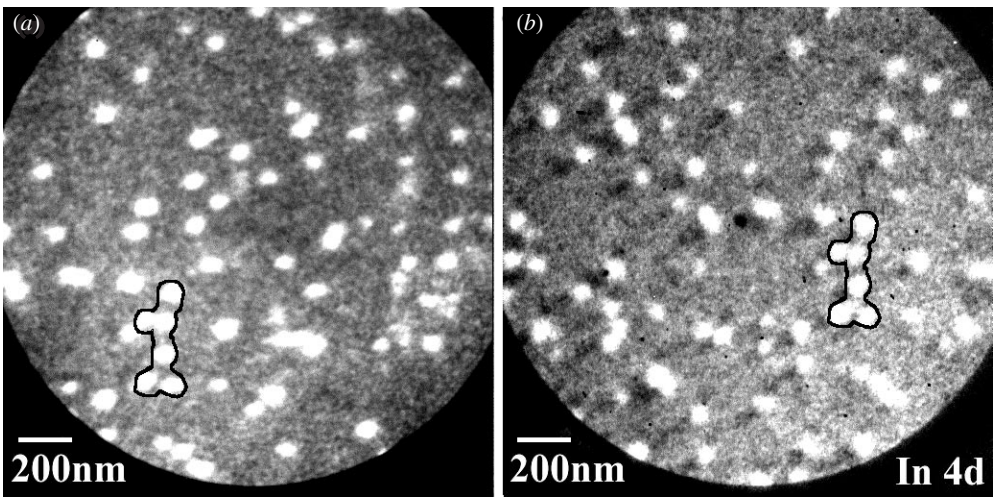

Figure 9. A LEEM image (*a*) and in 4d photoelectron XPEEM (*b*) image of InAs nanocrystals on a GaAs(100) surface. The number 1 indicates identical specimen positions [44].

5. Summary and outlook

The brief description of the principles, the instrumentation and the few selected application examples should give a general idea of the present state of photoelectron microscopy with synchrotron radiation. XPEEM has already made significant contributions to fundamental understanding and practical applications, mainly in the field of magnetism, but they stem from only a few groups with good instruments and sufficient access to high-brightness beamlines. The recent and ongoing construction of dedicated beamlines for XPEEM, the increasing number of good instruments and the development of aberration-corrected instruments should lead to considerable progress in this field in the near future.

Acknowledgments

The activities of the author in the field of magnetic microscopy are in part supported by the National Science Foundation under grant number DMR-818296, in part by ELETTRA and in part by NATO.

References

[1] Harp G and Tonner B P 1988 *Rev. Sci. Instrum.* **59** 853
Tonner B P and Harp G R 1989 *J. Vac. Sci. Technol.* A **7** 1
[2] Scholl A *et al* 2000 *Science* **287** 3973
[3] Bauer E 1978 *Leopoldina Symp. on Physik und Chemie der Kristalloberflaeche (Halle, DDR)* unpublished
[4] Bauer E and Telieps W 1988 *Surface and Interface Characterization by Electron Optical Methods* ed A Howie and U Valdre (New York: Plenum) p 195
[5] Bauer E 1994 *Rep. Prog. Phys.* **57** 895
[6] Bauer E 1998 *Surf. Rev. Lett.* **5** 1275
[7] Bauer E, Franz T, Koziol C, Lilienkamp G and Schmidt T 1997 *Chemical, Structural and Electronic Analysis of Heterogeneous Surfaces on the Nanometre Scale* ed R Rosei (Dordrecht: Kluwer) p 75
[8] Bauer E 1991 *Ultramicroscopy* **36** 52
[9] Anders S *et al* 1999 *Rev. Sci. Instrum.* **70** 3973
[10] Seah M P and Dench W A 1979 *Surf. Interf. Anal.* **1** 2
[11] Siegmann H C 1994 *Surf. Sci.* **307–9** 1157 and references therein
[12] Hong J and Mills D L 1999 *Phys. Rev.* B **59** 13 840 and references therein
[13] Stoehr J *et al* 1993 *Science* **259** 658
[14] Tonner B P *et al* 1994 *Nucl. Instrum. Methods Phys. Res.* A **347** 142
[15] Schneider C M *et al* 1993 *Appl. Phys. Lett.* **63** 2432
[16] Schneider C M *et al* 1994 *J. Phys.: Condens. Matter* **6** 1177
[17] Daimon H *et al* 2001 *Surf. Sci.* **471** 143
[18] Daimon H 2001 *Phys. Rev. Lett.* **86** 2034
[19] Kiskinova M *et al* 1999 *Surf. Rev. Lett.* **6** 265 and references therein
[20] Kiskinova M *et al* 2000 *Surf. Interf. Anal.* **30** 464 and references therein
[21] ELMITEC Elektronenmikroskopie GmbH: www.elmitec-gmbh.com
[22] Omicron Vakuumphysik GmbH: www.omicron-instruments.com
[23] Staib Instruments: www.staib-instruments.com
[24] De Stasio G *et al* 1998 *Rev. Sci. Instrum.* **69** 2062
[25] Schmidt Th *et al* 1998 *Surf. Rev. Lett.* **5** 1287
[26] Wichtendahl R *et al* 1998 *Surf. Rev. Lett.* **5** 1249
[27] Schmidt Th *et al* 2001 *Surf. Rev. Lett.* at press
[28] Sasaki S 1994 *Nucl. Instrum. Methods Phys. Res.* A **347** 87
[29] Young A T *et al* 1996 *J. Vac. Sci. Technol.* B **14** 3119
[30] Drescher M *et al* 1997 *Rev. Sci. Instrum.* **68** 1939
[31] Quitmann C *et al* 2001 *Surf. Sci.* **480** 173
[32] Agui A *et al* 2001 *Rev. Sci. Instrum.* **72** 3191
[33] Preikszas D 1995 *PhD Thesis* TU Darmstadt

[34] Kuch W *et al* 2000 *Phys. Rev.* B **62** 3824 and references therein
[35] Kuch W *et al* 2000 *J. Electron Spectrosc. Relat. Phenom.* **109** 249
[36] de Stasio G *et al* 2001 *Cancer Res.* **61** 4272
[37] Stoehr J *et al* 1998 *Surf. Rev. Lett.* **5** 1297
[38] Nolting F *et al* 2000 *Nature* **405** 767
[39] Ohldag H *et al* 2001 *Phys. Rev. Lett.* **86** 2878
[40] Locatelli A *et al* 2001 *Surf. Rev. Lett.* at press
[41] Shinjo T *et al* 2000 *Science* **289** 930
[42] Chen C T *et al* 1995 *Phys. Rev. Lett.* **75** 152
[43] Merkel M *et al* 2001 *Surf. Sci.* **480** 196
[44] Heun S *et al* 2001 *Phys. Rev.* B **63** 125335
[45] Bauer E 2001 *J. Electron Spectrosc. Relat. Phenom.* **114–6** 975
[46] Bauer E and Schmidt Th 2001 *High Resolution Imaging and Spectroscopy* ed M Ruehle and F Ernst (Berlin: Springer)